SCIENCE CHINA
Technological Sciences

•Article•

January 2023 Vol.66 No.1: 13–23
https://doi.org/10.1007/s11431-022-2232-5

Puncture site decision method for venipuncture robot based on near-infrared vision and multiobjective optimization

HE TianBao†, GUO ChuangQiang† & JIANG Li*

State Key Laboratory of Robotics and System, Harbin Institute of Technology, Harbin 150001, China

Received July 27, 2022; accepted October 12, 2022; published online December 12, 2022

Venipuncture robots have superior perception and stability to humans and are expected to replace manual venipuncture. However, their use is greatly restricted because they cannot make decisions regarding the puncture sites. Thus, this study presents a multi-information fusion method for determining puncture sites for venipuncture robots to improve their autonomy in the case of limited resources. Here, numerous images have been gathered and processed to establish an image dataset of human forearms for training the U-Net with the soft attention mechanism (SAU-Net) for vein segmentation. Then, the veins are segmented from the images, feature information is extracted based on near-infrared vision, and a multiobjective optimization model for puncture site decision is provided by considering the depth, diameter, curvature, and length of the vein to determine the optimal puncture site. Experiments demonstrate that the method achieves a segmentation accuracy of 91.2% and a vein extraction rate of 86.7% while achieving the Pareto solution set (average time: 1.458 s) and optimal results for each vessel. Finally, a near-infrared camera is applied to the venipuncture robot to segment veins and determine puncture sites in real time, with the results transmitted back to the robot for an attitude adjustment. Consequently, this method can enhance the autonomy of venipuncture robots if implemented dramatically.

puncture site decision, vein extraction, near-infrared vision, venipuncture robot

Citation: He T B, Guo C Q, Jiang L. Puncture site decision method for venipuncture robot based on near-infrared vision and multiobjective optimization. Sci China Tech Sci, 2023, 66: 13–23, https://doi.org/10.1007/s11431-022-2232-5

1 Introduction

Venipuncture is vital in medical procedures, such as drug delivery, blood collection, and physiological status monitoring [1]. Failed or delayed venipuncture may increase morbidity and death rates [2]. The success rate of venipuncture depends on the physiological characteristics of the patient and the expertise and competence of the clinical staff. Statistically, ~20% of venipunctures fail, which is serious for patients with difficult-to-identify veins, hairy or dark complexion, and other medical conditions [3,4]. Owing to the increasing demand for venipuncture, it is challenging to serve numerous patients promptly with limited medical resources [5].

With the advancements in medical robotics, it is anticipated that robots can perform venipuncture successfully. This ability is beneficial for decreasing venipuncture dependency on the expertise and skill of the clinical staff, as well as increasing the success rate. Meanwhile, such robots may also alleviate the strain on medical resources and reduce cross-infection when COVID-19 is still rampant. Although venipuncture robots are still mainly being developed, investigations have proved their superior vein detection capacities [6–8], motion planning abilities [7,9], and high success rates. To further improve the autonomy of the venipuncture robot under limited medical resources, it is critical to ensure that the robot can determine the puncture site.

Furthermore, decisions regarding the venipuncture site are based on the feature information of venous blood vessels;

†These authors contributed equally to this work.
*Corresponding author (email: jiangli01@hit.edu.cn)

hence, venous blood vessels must be segmented and extracted first from images. Deep-learning-based image segmentation achieves superior segmentation accuracy and generalization performance than traditional digital image processing techniques. However, this method is currently understudied for vein vascular segmentation. Chen et al. [8,10] initially used the recurrent fully convolutional network (Rec-FCN) for forearm venous vessel segmentation and obtained an accuracy of 84.3%. However, the results obtained were blurry and insensitive to the image details because the Rec-FCN network uses the sum of corresponding points when performing feature fusion [11]. Ji et al. [12] proposed a novel neural network (Mixer-UNet) for automated vein segmentation and recognition and achieved a segmentation accuracy of 93.07%. Also, these studies skeletonized the vessels when extracting veins, considered only their position information, and ignored the geometric information features of the vessels [13,14]. Incomplete vascular feature information cannot meet the needs of puncture site decision-making.

There are very few related studies on autonomous decision-making in venipuncture robots. In robotic venipuncture, the vascular puncture events can be detected using force, tactile, impedance, and ultrasound methods, but the puncture site must still be selected manually [15–18]. After the venous imaging, all existing robots rely on inputs from the clinical staff to select the puncture location, after which the robots perform the puncture. Although Chen et al. [8] suggested an approach for selecting puncture locations in 2013, they did not specify the implementation method of the strategy. Furthermore, the puncture sites were still selected manually in all their subsequent studies. Zhao et al. [19] proposed a puncture point decision algorithm based on connected domain identification, which selects the barycenter of the connected domain corresponding to the straight line intersecting the most connected domain sets as the target puncture point. However, this method only considers the curvature of the vessel and cannot fully meet the selection requirements of the puncture site.

Decisions regarding the puncture site must be evaluated using multiple interdependent criteria. First, the curvature of the vessel must be considered. An overly curved vessel causes difficulties in inserting the needle tip into the vessel entirely and can easily damage the vessel, leading to severe repercussions, such as tissue injury and drug penetration. Meanwhile, the cross-sectional size of the vessel must also be considered, and the cross-sectional change should be as small as possible along the length of the puncture needle entry. Additionally, the insertion angle of the needle significantly affects the puncture site. For instance, higher insertion angles have stricter requirements for the minimum diameter of the puncture site. In contrast, lower insertion angles have stricter requirements for the maximum length of the needle entry that the vessel can accommodate. Consequently, selecting the puncture site necessitates thoroughly evaluating the interactions between multiple parameters.

This study introduces a multi-information fusion method based on near-infrared (NIR) vision and multiobjective optimization to identify the optimal puncture site for a venipuncture robot. The method comprehensively considers the characteristic information of blood vessels. Primarily, an NIR imaging system is used to obtain the distribution image of the venous blood vessels, and the veins are segmented using a deep-learning model to ensure that the decision input data are accurate and reliable. In our previous study, we created a dataset for arm vein segmentation and segmented the vessels using SAU-Net [20]. Herein, this dataset is augmented from the previous research to improve the model's generalization performance, and we extract vascular features after vein segmentation. Additionally, the method is based on multiobjective optimization and employs image data segmented by deep learning as the input to determine the optimal puncture site for each vessel. Meanwhile, the puncture sites of multiple vessels in the same arm are filtered based on the interindividual dominance relationship to determine the optimal puncture site globally.

The remainder of this paper is structured as follows: Section 2 provides an overview of the method. Sections 3 and 4 introduce the methods for preliminary vessel selection and the optimal puncture site determination of the venipuncture, respectively. Sections 5 and 6 describe the experiments and outcomes, as well as their discussions. Finally, Section 7 concludes the study.

2 Methods

A self-designed venipuncture robot was used for vein detection, puncture status sensing, and target position movement. The robot recognizes blood vessels using a NIR camera and judges the punctured state based on the force between the needle and the tissue. The robot's six degrees of freedom permit positioning in the required workspace while altering the needle's attitude based on vein information. In the workflow of the venipuncture robot, autonomous determination of the puncture site is crucial for increasing the autonomy of the robot.

The method proposed herein to determine the puncture site is based on the vessel imaging data. Since the NIR light can improve the contrast between vessels and other tissues, it is advantageous for the robot to identify veins using the NIR light. Therefore, the NIR camera and light source image the veins to improve their visibility. Then, the veins are segmented with the SAU-Net model comprising the soft attention mechanism. The geometric features of each vein are extracted, including the location, curvature, and cross-sec-

tional size. Because the circle can adequately approximate the cross-section of the vessel, the cross-sectional information is reduced to the diameter. When determining the puncture site, it must be acknowledged that several criteria are not independent. For example, within a particular length of the vessel, the cross-sectional size may satisfy the venipuncture requirement, but the curvature of the vessel may be excessive, or the cross-sectional size may fluctuate significantly. Consequently, a multiobjective optimization model is presented to determine the puncture site, and the NSGA-II algorithm is applied to determine the ideal puncture site based on the vessel data.

As depicted in Figure 1, the site determination approach for the venipuncture robot introduced here comprises three steps: (1) vein segmentation, which entails preprocessing and segmenting the vein images acquired by the NIR imaging system; (2) feature extraction, which entails extracting and calculating the location information, curvatures, and diameters of the vessels for preliminary vessel selection for puncture; (3) optimization decision, which entails using the multiobjective optimization to calculate the solution set of puncture sites for each vessel and to choose the best puncture site globally.

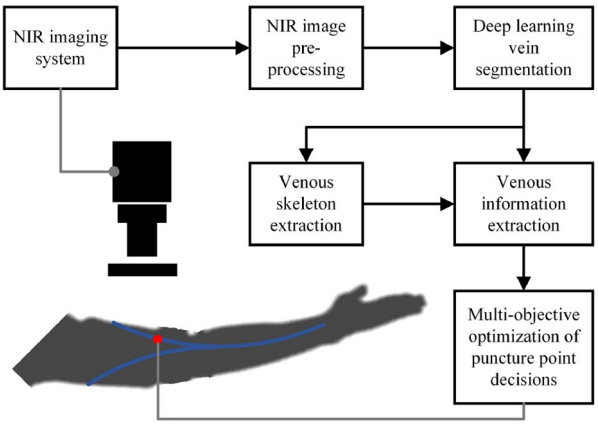

Figure 1 (Color online) Puncture site decision process.

3 Preliminary selection of venous vessels based on NIR vision

First, suitable vessels are selected for venipuncture. The veins are imaged using the NIR camera and light source, and their position is established by identifying oxyhemoglobin and deoxyhemoglobin contents. Owing to light scattering and attenuation, vessels with relatively large quantities of hemoglobin are recognized. Vessels with larger cross-sections closer to the surface are ideal for superficial venipuncture. Additionally, shorter vessels are filtered out during information extraction, providing a filter for vessels acceptable for venipuncture.

3.1 Vein segmentation

Figure 2 demonstrates the SAU-Net model with the soft attention mechanism applied to segment the veins. The encoder extracts the feature using convolutional down-sampling, whereas the decoder accomplishes same-scale fusion using deconvolutional up-sampling to restore the image details and spatial dimensions gradually. During up-sampling restoration, the features propagated by skip connections after soft attention processing are added to the classical U-Net [6,21]. This addition helps the model assign weights to each part of the input image, extract critical information, suppress other useless information, and achieve multiscale feature recognition to improve the segmented edge accuracy. This reduces the training and image segmentation times of the model and improves the vein segmentation performance in real time [22,23]. Our earlier study [20] describes this model comprehensively.

Labeled training data are required for learning supervised algorithms. Unfortunately, there is no publicly available dataset for arm vein images, so the digital arm images for vein segmentation dataset was established [20]. This dataset was expanded herein to enhance the number and quality of images. The enlarged dataset uses four NIR cameras (two cameras of GS3-U3-41C6NIR-C, FLIR systems, Alabama, United States, and two cameras of 1800 U-501m mono NIR S-Mount, Allied Vision, Stadtroda, Germany) to acquire arm vein images of volunteers under various lighting conditions (natural light, NIR filtering, and 850-nm NIR light) to strengthen the flexibility of the model for different populations and environments. Ground truth images of the arm veins were then obtained by expert annotation of the dataset images (Figure 3).

3.2 Vein feature extraction

Location, diameter, and curvature are some of the properties of the vessel. Since the forearm has several intersecting vessels, these vessels must be isolated first. The algorithm for vessel extraction is shown in Algorithm 1. When extracting blood vessels, the skeleton of the vessels is computed first. Next, the image is normalized, and the pixels are assigned values 0 (background) and 1 (veins). As shown in Figure 4(a), the attributes of each point are identified by calculating the sum of the eight neighbors of each pixel. Once a judgment is rendered, each point is revised to a background point to prevent repeated judgment. For example, if the sum of the neighbors is 2, the point represents the vessel's center. If the sum of the neighbors exceeds 2, the point represents the vessel's intersection. Furthermore, if the sum of the neighbors is 0, the point represents the vessel's

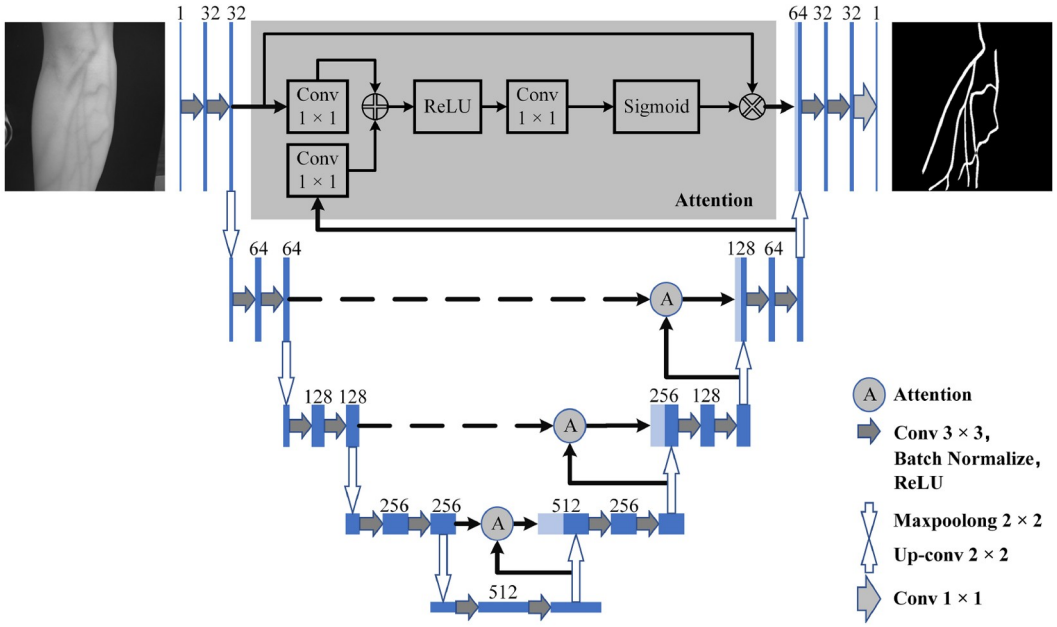

Figure 2 (Color online) Deep-learning-based vein segmentation model SAU-Net.

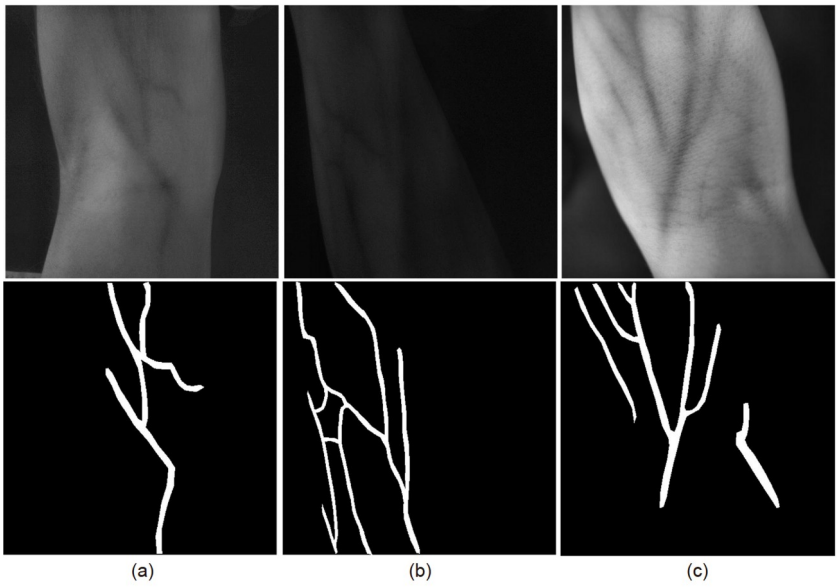

Figure 3 Some samples of the dataset. (a) Arm images under (a) natural light, (b) NIR filtering, and (c) 850-nm NIR light enhancement.

termination or an isolated point. Finally, the set of vessel location points is obtained.

The curvature and diameter of the vessel are computed after extracting the position. The curvature of the vessel is defined as the degree to which its angle varies throughout a given length. The vessel's angle is defined as the acute angle of a line between two neighboring points rotated in the vertical direction, with the counterclockwise and clockwise directions being positive and negative, respectively (Figure 4 (b)). The computed diameter of the vessel is not the actual diameter but rather the number of pixels in the radial direction.

4 Multiobjective-optimization-based puncture location decision method

4.1 Optimization variables and objective functions

The puncture site decision is a multiobjective optimization problem with a model comprising three components: opti-

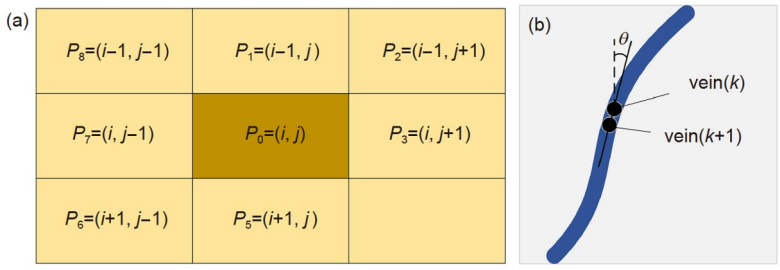

Figure 4 (Color online) (a) Eight neighbors of a pixel and (b) angle of the vessel.

Algorithm 1 Extracting veins from the image

1: **Input**: Vein skeleton image I
2: Initialize: num=0, k=0
3: I_N =normalize(I)
4: **while** sum(I_N[0:m, 0:n])>0 **do**
5: [i,j]←argmax (I_N[0:m, 0:n])
6: p_0←[i,j]
7: $I_N[p_0]$←0
8: vein[k]←p_0
9: k←k+1
10: compute p[1,2,…,8] of p_0
11: **if** sum($I_N[p_1,p_2,\ldots,p_8]$=1) **then**
12: p_0← argmax $I_N[p_1,p_2,\ldots,p_8]$
13: **else**
14: veins[num]←vein
15: num←num+1
16: k←0
17: **end if**
18: **end while**
19: **Output**: positions of all veins in the image

mization variables, objective function, and constraints. In this approach, the optimal puncture site within the vein is the decision goal. Therefore, the optimization variable for this problem is the vessel's point. The optimization variable is given as follows:

$$\mathbf{P}=\begin{bmatrix}\mathbf{P}_1\\ \mathbf{P}_2\\ \vdots\\ \mathbf{P}_n\end{bmatrix}=\begin{bmatrix}x_1 & y_1 & d_1 & a_1\\ x_2 & y_2 & d_2 & a_2\\ \vdots & \vdots & \vdots & \vdots\\ x_n & y_n & d_n & a_n\end{bmatrix}, \tag{1}$$

where $\mathbf{P}_i$ is the vein information at the ith point, (x_i, y_i) is the ith point position, and d_i and a_i are the vein diameter and angle at the ith point, respectively.

First, the radial requirements of the puncture site are considered. The diameter of the vessel must allow a fixed length of the needle to enter—besides, the thicker the vessel, the lower the danger of puncture. Also, the vessel will be distorted by force because of the elasticity of soft tissues, and the vessel deformation should be minimal in the radial direction. The radial deformation of the vessel in the elastic force range is inversely proportional to its cross-sectional area. Consequently, the radial objective function is given as follows:

$$F_R=a_1\sum_{i=j}^{j+N-1}\frac{\boldsymbol{\lambda}_i\mathbf{P}_i^{\mathrm{T}}}{N}+a_2\sum_{i=j}^{j+N-1}\frac{\left(\boldsymbol{\lambda}_i\mathbf{P}_i^{\mathrm{T}}\right)^2}{N}. \tag{2}$$

In the axial direction of the vessel, the changes in the vessel diameter and curvature within a specified distance of the target position must be considered. To avoid abrupt changes in the cross-sectional dimensions of the vessel, the vessel diameter should be uniform over its length. Similarly, the vessel curvature should be as slight as feasible, i.e., the straighter the vessel, the more suitable it is for venipuncture to minimize the risk of puncturing the vessel and damaging the surrounding tissues. Therefore, the axial objective function is given as follows:

$$F_A=b_1\sum_{i=j}^{j+N-1}\sqrt{\left(\boldsymbol{\lambda}_i(\mathbf{P}_i-\mathbf{P}_{i+1})^{\mathrm{T}}\right)^2}+b_2\sum_{i=j}^{j+N-1}\sqrt{\left(\boldsymbol{\tau}_i(\mathbf{P}_i-\mathbf{P}_{i+1})^{\mathrm{T}}\right)^2}, \tag{3}$$

where j is the vein point index, and $j=1,2,...,n-N$. Also, a_1, a_2, b_1, and b_2 are the weighting factors. $\boldsymbol{\lambda}_i=[0\ \ 0\ \ \lambda\ \ 0]$ is the decision variable associated with the vessel diameter, and $\boldsymbol{\tau}_i=[0\ \ 0\ \ 0\ \ \tau]$ is the decision variable from the vascular perspective. When point i is selected in the range $[i,i+N)$, $\lambda=1$ and $\tau=1$, otherwise $\lambda=0$ and $\tau=0$, such that

$$\boldsymbol{\lambda}_i(\mathbf{E}-\boldsymbol{\lambda}_i)^{\mathrm{T}}=\boldsymbol{\tau}_i(\mathbf{E}-\boldsymbol{\tau}_i)^{\mathrm{T}}=0. \tag{4}$$

N is the length of the vessel to be considered for the target points in the image, i.e., the number of pixels:

$$N=\sum_{i=1}^{i=n}\|\boldsymbol{\lambda}_i\|_1=\sum_{i=1}^{i=n}\|\boldsymbol{\tau}_i\|_1. \tag{5}$$

4.2 Constraints

Imaging the human elbow revealed that the veins are primarily dispersed along the axial direction of the arm. At the intersection of the two vessels, there may be an almost radial

connection. Additionally, this portion of the vessel is either too bent or narrow in diameter to permit venipuncture. Consequently, to reduce the optimization decision time, the range of the average angle $\overline{\theta}$ of the vessels within the target length is set to $[-45°, 45°]$, i.e.,

$$\tan^2(\overline{\theta}) \geqslant 1. \tag{6}$$

Since the specific length of the needle must enter the vessel, features within the target length of the puncture site must be considered. This length range depends on the dimensional characteristics of the needle and the insertion angle. During the puncture, a smaller insertion angle requires a more significant vessel length L to prevent the needle from puncturing the vessel axially. Conversely, a larger insertion angle requires a larger vessel diameter C to prevent the needle from puncturing the distal vessel wall.

$$N > L = g_1(l_{\text{needle}}, \alpha) = g_{1,\min(\alpha)}(l_{\text{needle}}) = 0.7 l_{\text{needle}}. \tag{7}$$

Also, it is necessary to consider the minimum value of the vessel diameter within the target length of the puncture point, i.e.,

$$\boldsymbol{\lambda}_i \mathbf{P}_i^{\mathrm{T}} > C = g_2(d_{\text{needle}}, \alpha) = g_{2,\max(\alpha)}(d_{\text{needle}}) = 3 d_{\text{needle}}, \tag{8}$$

where L and C are functions related to the needle length l_{needle}, diameter d_{needle}, and feed angle α. Thus, the optimization model of the puncture site decision for the robot is

$$\begin{aligned}
&\max F_R = a_1 \sum_{i=j}^{j+N-1} \frac{\boldsymbol{\lambda}_i \mathbf{P}_i^{\mathrm{T}}}{N} + a_2 \sum_{i=j}^{j+N-1} \frac{\left(\boldsymbol{\lambda}_i \mathbf{P}_i^{\mathrm{T}}\right)^2}{N}, \\
&\min F_A = b_1 \sum_{i=j}^{j+N-1} \sqrt{\left(\boldsymbol{\lambda}_i (\mathbf{P}_i - \mathbf{P}_{i+1})^{\mathrm{T}}\right)^2} \\
&\quad + b_2 \sum_{i=j}^{j+N-1} \sqrt{\left(\boldsymbol{\tau}_i (\mathbf{P}_i - \mathbf{P}_{i+1})^{\mathrm{T}}\right)^2}, \\
&\quad s.t.\ \tan^2\left(\overline{\theta}^{\mathrm{D}}\right) > 1, \\
&\quad N > L = g_1(l_{\text{needle}}, \alpha), \\
&\quad \boldsymbol{\lambda}_i \mathbf{P}_i^{\mathrm{T}} > C = g_2(d_{\text{needle}}, \alpha).
\end{aligned} \tag{9}$$

4.3 Optimization method

The proposed procedure for multiobjective optimization coordinates the relationship between each objective function and discovers the solution set that maximizes the optimal value of each objective function. However, the objectives are mutually restricted. Consequently, a target may be enhanced at the expense of others, and there is no ideal solution that maximizes the performance of all objectives. Consequently, the solution to the multiobjective optimization problem is typically a collection of noninferior options, also known as the Pareto solution set.

Two objective functions were applied to the radial and axial demands of the vessel in the model for puncture location. Therefore, the genetic algorithm for undominated ranking with an elite strategy (NSGA-II) was employed [24–26]. This method mixes the parent and offspring populations to build the next-generation population through competition while preserving the best individuals by storing them hierarchically. This approach ensures that the best individuals are not lost to evolution and can rapidly increase the population level, thereby boosting the precision of the optimization outcome. Meanwhile, to facilitate this solution, the maximization problem is transformed into a minimization problem in the optimization. Additionally, considering that the venipuncture site is equally critical for axial and radial requirements, the two objective functions are assigned the same weights.

5 Experimental methods and results

5.1 Vein segmentation and feature extraction

During model training, the dataset was augmented. Because medical photos entail personal privacy and are costly, the dataset is limited. To prevent model underfitting caused by minimal data, the dataset was augmented to 1376 sets via size expansion, random cropping, and random flipping before model training. The training and test sets were divided into a 7:3 ratio. The initial learning rate was set to 0.001 and decreased by 0.2 when the reference evaluation measure ceased to improve or the model failed to develop for five consecutive epochs.

The model segmentation accuracy was 91.2%, sensitivity was 92.3%, and the area under the receiver operating characteristic (ROC) curve was 0.945%. Figure 5 depicts the ROC and precision-recall (PR) curves. Compared to expert segmentation findings for the left and right arms of 10 students (n=20), the SAU-Net model detected 86.3% (101/117) of the veins. Additionally, the dice score (mean value=0.865 ±0.512) for each picture model segmentation exceeds 0.8.

The position, diameter, and curvature of each vein were derived from the segmented vein images. Also, the segmentation results were filtered for veins with short lengths and small diameters. The number of venous vessels extracted by the model and the actual number of vessels in Figure 6(a) are 5/7, 4/6, 5/6, and 4/5. These results are presented in Figure 6 (b) and (c).

5.2 Puncture site decision

The extracted vessel information was used as the decision for each vessel in the optimization model for puncture site decision. Meanwhile, the NSGA-II was used to calculate the optimization. Binary coding was used because of the discrete nature of the variables, and genetic operations are simple to

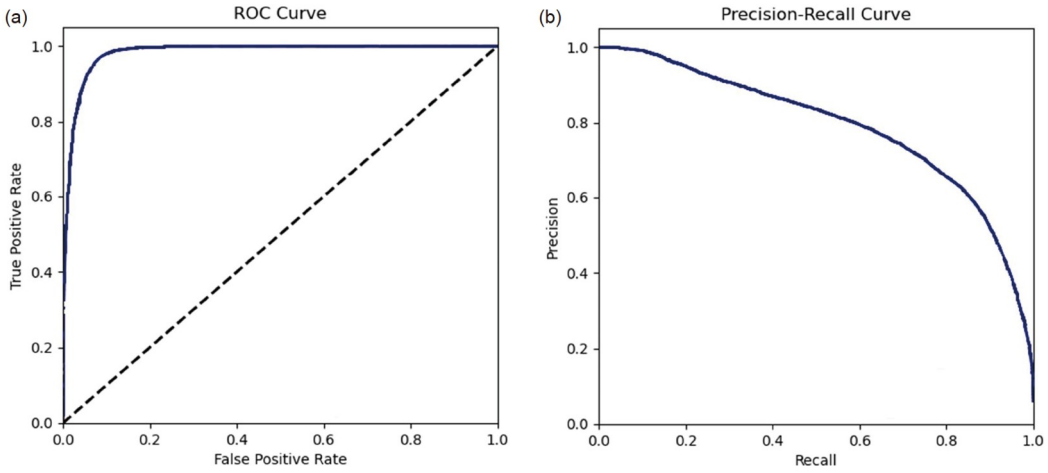

Figure 5 (Color online) ROC curve (a) and PR curve (b).

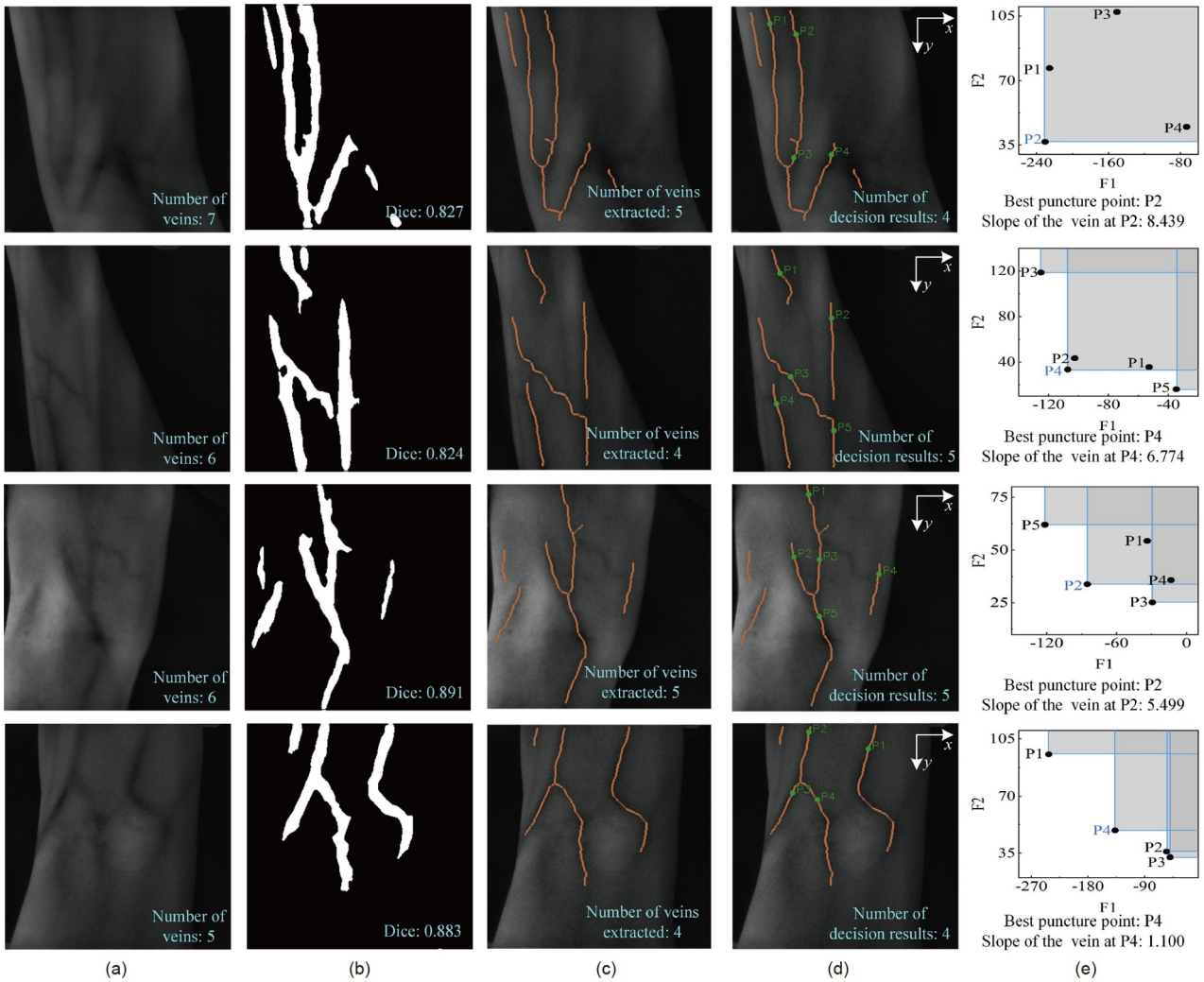

Figure 6 (Color online) Puncture decision results. (a) Original image; (b) vein segmentation; (c) vein extraction; (d) puncture site decision; (e) global optimal result.

execute. Furthermore, the number of population members was fixed at 30. The crossover and variation probability values were set to 0.7 and 1/20, and the maximum number of evolutionary generations was set to 300. Also, the type,

diameter d_{needle}, and length l_{needle} of the standard needle used in venipuncture were counted. Considering the range of the needle entry angles from 10° to 30° for venipuncture, the estimated safe diameter C=3d_{needle}, and safe insertion length L=0.7l_{needle} for different models of needles are presented in Table 1. To enhance the safety of the decision site, the safe diameter and insertion length were calculated using an approach angle of 30° and 10°, respectively.

Since multiple vessels exist in each image, the decision result for each vessel (average decision time=1.458 s) has the best set of solutions. The best solution for each vessel was filtered by considering two objective functions for the decision results of all vessels in a balanced manner.

Each vessel has a different number of Pareto solution sets (Figure 6(d)). Some vessels have several puncture decision sites, whereas others lack a puncture decision site that fits the criteria. For an individual's vessel puncture solution sets, the F1–F2 plot for each solution was drawn (with the values F1 and F2 of objective functions one and two as the horizontal and vertical coordinates, respectively). The final puncture decision results were obtained by considering the dominant relationships between the solution sets (Figure 6(e)). After collecting the coordinates of the vein whose length exceeded L according to the final result, the slope at the puncture site was fitted.

Considering that the most common venipuncture needle size for humans is 22G, all trials in this investigation were conducted for this parameter. The average diameters of the four choice results displayed in Figure 6(e) over the length range L are 2.854, 3.195, 2.982, and 3.586 mm, with the standard deviation of the diameter being < 0.050 mm.

5.3 Robot position and attitude adjustment based on puncture site decision

Experiments on the puncture site determination were conducted using the self-developed six-degrees-of-freedom venipuncture robot to modify the needle position and attitude.

Table 1 Parameters of the puncture needles

Type	24G	23G	22G	21G	20G
d_{needle} (mm)	0.55	0.60	0.70	0.80	0.90
l_{needle} (mm)	20	24	25	26	27
C (mm)	1.5	1.8	2.1	2.4	2.7
L (mm)	14	17	18	19	19

The ranges of motion of the robot are 70, 80, and 40 mm in the x, y, and z directions in a three-dimensional (3D) space, respectively. The positioning accuracy values are 0.08, 0.05, and 0.07 mm, and the repeatability values are 0.03, 0.02, and 0.02 mm, respectively. The *yaw*, *pitch*, and *inj* axes have ranges of motion from −45° to 45°, 0° to 30°, and 0 to 16 mm, and the repeatability values are 0.03°, 0.06°, and 0.03 mm, respectively. The end effector of the robot can retain the needle tip at the intersection of the *yaw* and *pitch* axes before puncturing (Figures 7(a) and (b)). Therefore, the needle tip position remains unchanged when the needle posture is adjusted. Also, both the end effector and camera (1800 U-501m mono NIR S-Mount, Allied Vision) are installed on the robotic-positioning arm (Figure 7(a)). The positions are relatively fixed, and the calibration is completed [27,28], so the needle tip position in the image remains unchanged during movement. The software system of the robot is written in Python and QT to realize the vein image processing, puncture decision, and robot motion control.

In this experiment, the NIR camera captured real-time images of the arm veins to determine the optimal puncture site. The final result of the puncture decision includes the pixel coordinates of the puncture site and vein angle. The site information was transformed to the robot's coordinate system position, and the robot moved to the puncture site accordingly. The robot simultaneously adjusts its *yaw* angle (i.e., the angle between the needle and numerical direction) following the vessel angle such that the needle is parallel to the vessel at the puncture site (Figure 7(c)).

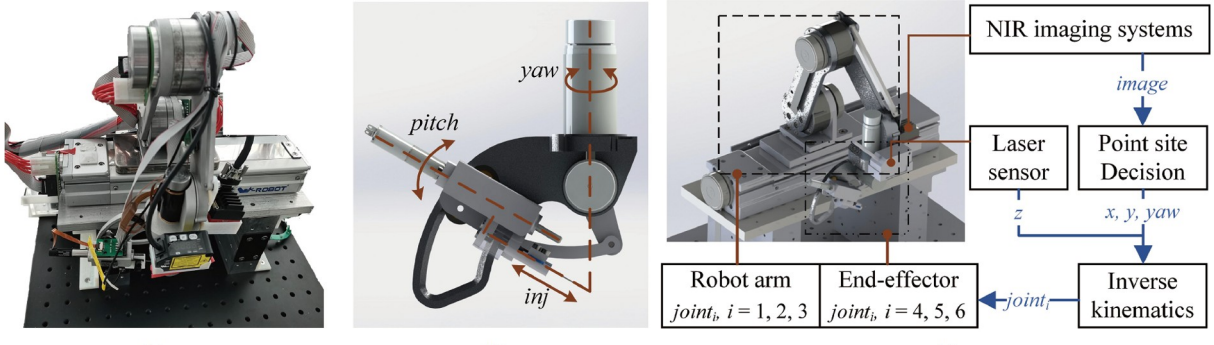

Figure 7 (Color online) Experimental platform. (a) Venipuncture robot; (b) *yaw* and *pitch* axes of the robot; (c) process of robot positioning and attitude adjustments based on the puncture site decision.

The errors in the robot's movement to the puncture position in the x and y directions are <0.100 and 0.050 mm, respectively, and the *yaw* angle error is < 0.050°. The experimental results are illustrated in Figure 8. The location of the puncture point is (186.049, 189.666), and the angle is 10.930° (Figure 8(a)). The robot's initial position and *yaw* angle are (149.867, 159.634) and 29.885°, respectively (Figure 8(b)). When the robot reaches the puncture point, the needle tip is located at (185.998, 189.676), with a *yaw* angle of 10.958°. The errors relative to the target position are 0.052 and 0.010 mm in the x and y directions, respectively, and 0.028° along the *yaw* axis. Figure 8(c) shows the relative positional changes of the needle and puncture point during the experiment, with the red rectangle and bright yellow dot indicating the needle's position and the target location, respectively. During movement, the location and attitude are simultaneously modified.

6 Discussion

This study presents a method for autonomous puncture site decision-making for the venipuncture robot based on the SAU-Net model and multiobjective optimization. The results demonstrate that deep-learning-based vein segmentation and feature extraction can efficiently extract veins and that the multiobjective-optimization-based puncture site decision model can determine the optimal puncture site on the vein. Furthermore, the proposed method was applied to the venipuncture robot to adjust its position and attitude based on the ideal puncture site. This enables achieving more autonomous venipuncture under the supervision of clinical staff.

Initially, vessels with the most suitable depth, length, and diameter were screened using the NIR imaging system and vessel extraction algorithm. Because hemoglobin absorbs NIR light more strongly than other tissues, the NIR vision-based vein identification method can acquire more precise vessel positions. Concurrently, fuzzy, thin, and short vessels are filtered when vein segmentation and feature extraction are performed. Besides, only those vessels suitable for puncture location determination are screened. This eliminates decision interference, improves decision efficiency, and ensures the safety of the puncture site.

This study utilized the deep-learning-based approach for vein segmentation and feature extraction because puncture site decisions depend on the accuracy of vein information. Although studies have been conducted on retinal vessel segmentation [29,30] and vein segmentation based on the Rec-FCN [6], a dataset for training the segmented forearm vein model has not been developed. Therefore, this study presents a dataset for segmenting human forearm veins as a pioneering work. This dataset considers the impact of the equipment and environment on imaging. Besides, the images were obtained using four cameras in three circumstances to reduce the environmental interference on vein segmentation.

During making the puncture site decision, at least one vein suitable for robotic venipuncture should be extracted for a given patient, and the optimal puncture location can be calculated. During the experiments, the approach proposed herein can extract approximately four veins (86.3%), which exceeds the results of the manual evaluation (73.9%) and Rec-FCN detection (78.8%) [6].

Additionally, the multiobjective-optimization-based puncture site decision method fully considers the effects of the insertion angle, vessel size, degree of curvature, and needle size. The method optimizes decision-making sites for

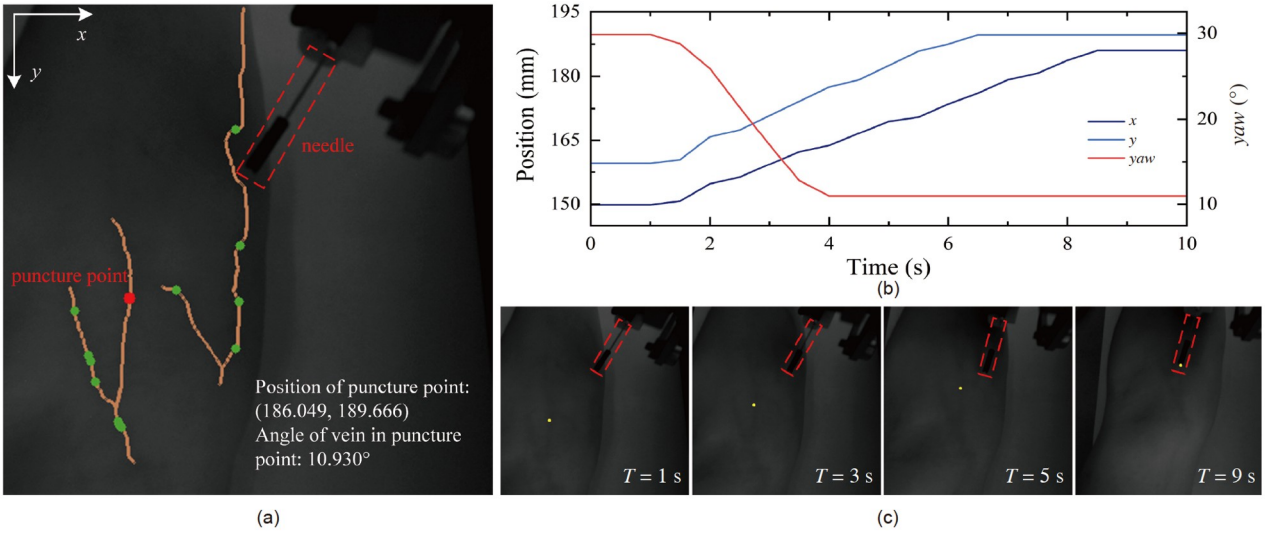

Figure 8 (Color online) Puncture site decision experiment with the robot. (a) Puncture decision results; (b) the robot adjusts the position and attitude of the needle according to the puncture site; (c) puncture site and relative position of the needle during robot movement.

each vessel and finally filters the optimal venous puncture location from multiple Pareto solution sets based on the value of the objective function. The information on the vessel's angle at the puncture position for the desired length is also provided, thus eliminating the manual selection of the puncture location by the clinical staff.

This work proposes an autonomous decision-making method for a venipuncture robot with multi-information fusion. It has been reported that most venipuncture robots require a manual selection of puncture sites by the clinical staff [6,9,31–33], which does not relieve the staff of venipuncture duties. In the experiments, the error between the target puncture point and the needle tip of the venipuncture robot was <0.100 mm. Moreover, the angle error between the needle and blood vessel was <0.050°, demonstrating that the method yields superior results to the venipuncture robot. Thus, the proposed method improves the autonomy of the venipuncture robot and enables the robot to accomplish tasks with less monitoring. However, it reduces the probability of puncture failure due to variations in the axes of the puncture needle and the vein.

7 Conclusion

This study presents a puncture site decision-making method with multi-information fusion for the automated venipuncture robot by utilizing vein images after SAU-Net network segmentation and feature extraction as the input information for optimal puncture site selection. In this work, vein segmentation and feature extraction experiments were conducted on ten humans, with an accuracy of 91.2% for segmentation and an extraction rate of 86.3% for the veins. The experiments indicated that multiple Pareto solution sets and an optimal puncture site could be calculated using the extracted venous information as the input to a multiobjective optimization model following the preliminary selection of vessels using NIR vision. Additionally, the approach viably provided the position and attitude data to the venipuncture robot. Furthermore, the results indicate that the proposed technology can be employed in clinical applications and has a high potential for automatic puncture site decision-making, along with providing the basis for improving the autonomy of other medical robots.

This work was supported by the National Natural Science Foundation of China (Grant No. U1813209) and Self-Planned Task of State Key Laboratory of Robotics and System (Harbin Institute of Technology) (Grant No. SKLRS202112B).

1 Horattas M C, Trupiano J, Hopkins S, et al. Changing concepts in long-term central venous access: Catheter selection and cost savings. Am J Infect Control, 2001, 29: 32–40
2 Sampalis J S, Lavoie A, Williams J I, et al. Impact of on-site care, prehospital time, and level of in-hospital care on survival in severely injured patients. J Trauma-Injury Infect Crit Care, 1993, 34: 252–261
3 Armenteros-Yeguas V, Gárate-Echenique L, Tomás-López M A, et al. Prevalence of difficult venous access and associated risk factors in highly complex hospitalised patients. J Clin Nurs, 2017, 26: 4267–4275
4 Lamperti M, Pittiruti M. Difficult peripheral veins: Turn on the lights. Br J Anaesthesia, 2013, 110: 888–891
5 Hulse E J, Thomas G O R. Vascular access on the 21st century military battlefield. J R Army Med Corps, 2010, 156: S385–390
6 Chen A I, Balter M L, Maguire T J, et al. Deep learning robotic guidance for autonomous vascular access. Nat Mach Intell, 2020, 2: 104–115
7 Chen A I, Balter M L, Maguire T J, et al. Real-time needle steering in response to rolling vein deformation by a 9-DOF image-guided autonomous venipuncture robot. In: Proceedings of 2015 IEEE/RSJ International Conference on Intelligent Robots and Systems (IROS). Hamburg, Germany: IEEE, 2015. 2633–2638
8 Chen A, Nikitczuk K, Nikitczuk J, et al. Portable robot for autonomous venipuncture using 3D near infrared image guidance. Technology, 2013, 1: 72–87
9 Balter M L, Chen A I, Maguire T J, et al. Adaptive kinematic control of a robotic venipuncture device based on stereo vision, ultrasound, and force guidance. IEEE Trans Ind Electron, 2017, 64: 1626–1635
10 Chen A I. Image-guided robotics for autonomous venipuncture. Dissertation for the Doctoral Degree. New Brunswick: Rutgers University. 2016. 25–28
11 Wang D H, Feng G L, Wang X, et al. Research on image segmentation algorithm based on features of venous gray value. Opto Electron Eng, 2018, 45: 180066
12 Ji J, Zhao Y, Xie T, et al. Automated vein segmentation from NIR images using a mixer-UNet model. In: Liu H, Yin Z, Liu L, et al., eds. Intelligent Robotics and Applications. Cham: Springer International Publishing, 2022. 64–75
13 Lin G, Wang H, Sha M, et al. Design of a Multi-data fusion intelligent venipuncture blood sampling robot. In: Proceedings of 2022 7th International Conference on Control and Robotics Engineering (ICCRE). Beijing, China: IEEE, 2022. 10–15
14 Sha M, Wang H, Lin G, et al. Design of multi-sensor vein data fusion blood sampling robot based on deep learning. In: Proceedings of 2022 2nd International Conference on Computer, Control and Robotics (ICCCR). Shanghai, China: IEEE, 2022. 46–51
15 Zivanovic A, Davies B L. A robotic system for blood sampling. IEEE Trans Inform Technol Biomed, 2000, 4: 8–14
16 Cheng Z, Davies B L, Caldwell D G, et al. A hand-held robotic device for peripheral intravenous catheterization. Proc Inst Mech Eng H, 2017, 231: 1165–1177
17 Kobayashi Y, Hamano R, Watanabe H, et al. Use of puncture force measurement to investigate the conditions of blood vessel needle insertion. Med Eng Phys, 2013, 35: 684–689
18 Zhuang Y, Chen J, Liu Q, et al. Preliminary study on mechanical characteristics of maxillofacial soft and hard tissues for virtual surgery. Int J CARS, 2021, 16: 151–160
19 Zhao Y, Ji J, Xie T, et al. Vessel site selection for autonomous cannulation under NIR image guidance. In: Liu H, Yin Z, Liu L, et al., eds. Intelligent Robotics and Applications. Cham: Springer International Publishing, 2022. 88–99
20 He T, Guo C, Jiang L, et al. Automatic venous segmentation in venipuncture robot using deep learning. In: Proceedings of 2021 IEEE International Conference on Real-Time Computing and Robotics (RCAR). Xining, China: IEEE, 2021. 614–619
21 Long J, Shelhamer E, Darrell T. Fully convolutional networks for semantic segmentation. In: Proceedings of 2015 IEEE Conference on Computer Vision and Pattern Recognition (CVPR). Boston: IEEE, 2015. 3431–3440
22 Ronneberger O, Fischer P, Brox T. U-Net: Convolutional networks for

biomedical image segmentation. arXiv: 150504597
23 Valipour S, Siam M, Jagersand M, et al. Recurrent fully convolutional networks for video segmentation. In: Proceedings of 2017 IEEE Winter Conference on Applications of Computer Vision (WACV). Santa Rosa: IEEE, 2017. 29–36
24 Jain H, Deb K. An evolutionary many-objective optimization algorithm using reference-point based nondominated sorting approach, Part II: Handling constraints and extending to an adaptive approach. IEEE Trans Evol Computat, 2014, 18: 602–622
25 Deb K, Jain H. An evolutionary many-objective optimization algorithm using reference-point-based nondominated sorting approach, Part I: Solving problems with box constraints. IEEE Trans Evol Computat, 2014, 18: 577–601
26 Deb K, Pratap A, Agarwal S, et al. A fast and elitist multiobjective genetic algorithm: NSGA-II. IEEE Trans Evol Computat, 2002, 6: 182–197
27 Li W L, Xie H, Zhang G, et al. Hand–eye calibration in visually-guided robot grinding. IEEE Trans Cybern, 2016, 46: 2634–2642
28 Wang G, Li W, Jiang C, et al. Simultaneous calibration of multi-coordinates for a dual-robot system by solving the AXB = YCZ problem. IEEE Trans Robot, 2021, 37: 1172–1185
29 Fu H, Xu Y, Wong D W K, et al. Retinal vessel segmentation via deep learning network and fully-connected conditional random fields. In: Proceedings of 2016 IEEE 13th International Symposium on Biomedical Imaging (ISBI). Prague: IEEE, 2016. 698–701
30 Al-Bander B, Williams B, Al-Nuaimy W, et al. Dense fully convolutional segmentation of the optic disc and cup in colour fundus for glaucoma diagnosis. Symmetry, 2018, 10: 87
31 Balter M L, Chen A I, Fromholtz A, et al. System design and development of a robotic device for automated venipuncture and diagnostic blood cell analysis. In: Proceedings of 2016 IEEE/RSJ International Conference on Intelligent Robots and Systems (IROS). Daejeon, South Korea: IEEE, 2016. 514–520
32 Balter M L, Chen A I, Maguire T J, et al. The system design and evaluation of a 7-DOF image-guided venipuncture robot. IEEE Trans Robot, 2015, 31: 1044–1053
33 Qiao Z, Li Y, Wu Z, et al. Automatic puncture system based on NIR image and ultrasonic image. In: Proceedings of International Conference on Mechanical, Aeronautical and Automotive Engineering (ICMAA). Malacca, 2017, 108: 15002